$\mathcal{H}_2$-Optimal Blending of Inputs and Outputs for Modal Control

Manuel Pusch, Daniel Ossmann

***Abstract*—For many dynamical systems it is required to actively control individual modes, especially when these are lightly damped or even unstable. In order to achieve a maximum control performance, these systems are often augmented with a large number of control inputs and measurement outputs. To overcome the challenge of choosing an adequate combination of input and output signals for modal control, an $\mathcal{H}_2$-optimal isolation of modes via blending of inputs and outputs is proposed in this article. Enforcing an explicit mode decoupling, the approach enables controlling individual modes with simple single-input single-output controllers. A numerically efficient algorithm is derived for the joint computation of the interdependent input and output blending vectors. The effectiveness of the proposed approach is demonstrated by increasing the modal damping of an aeroelastic system.**

***Index Terms*—mode decoupling, modal control, over-actuated and over-sensed systems**

I. Introduction

ADVANCES in sensing and actuation technology allow improving the performance and reliability of feedback control systems. For instance, sophisticated sensors like micro-electro-mechanical systems or fiber optical sensors enable a large number of highly accurate measurements at low cost [1], [2]. Similarly, smart materials based on, e.g., smart memory alloys or piezoelectric ceramics allow for a fast and precise control of mechanical structures like aircraft wings [3], [4]. The challenge arising thereby is that a large number of degrees of freedom is introduced which clearly complicates controller design.

To tackle this problem, well established multiple-input multiple-output (MIMO) control approaches aiming to minimize the closed-loop $\mathcal{H}_2$ or $\mathcal{H}_\infty$ norm may be used [5]. The resulting controller commonly has the same order as the synthesis model augmented with tunable weighting filters to impose closed-loop specifications. This means that if the number of inputs and outputs increases, typically the controller order and the number of free tuning parameters also increases. In practice, however, low-order controllers which are easy to tune are desired or even necessary for numerically stable controller design and tuning. To keep the controller order low, model order reduction routines may be applied on the (augmented) synthesis model or the controller itself, whereby closed-loop guarantees are commonly lost. As an alternative, controller gains may be optimized directly, where the challenge is to choose an adequate controller structure with a minimum number of free parameters.

In this article, a novel control approach is presented, which targets to directly control single modes of over-actuated and over-sensed systems with low-order single-input single-output (SISO) controllers. To handle the large number of inputs and outputs, it is proposed to isolate each target mode by blending inputs and outputs and thereby generate independent SISO control loops. This splits modal controller design in two separate but more intuitive and easier tunable parts. The overall order of the resulting controller sums up from the individual orders of the SISO controllers, which are typically of low order and tuned on the full-order model. Hence, performance losses or stability issues due to model order reduction are avoided effectively.

There is a rich literature on approaches for modal decoupling and modal control. To allow for a so-called modal space control, approaches based on state observers, as Kalman or Luenberger oberservers, are commonly used [6]. However, it has been acknowledged that the possibility of spillover effects is rather high, see [7], [8] for detailed discussions. Since observers are part of the controller and typically are of the same order as the plant, a minimum-order modal controller design is proposed in [9]. Similarly, simply structured controllers for dynamic mode decoupling are derived in [10] using a linear matrix inequality formulation. In comparison to these *dynamic* decoupling approaches, *static* mode decoupling does not add states, but requires a sufficient number of inputs and outputs. See [11] for necessary conditions for full mode decoupling and [12], [13] for respective applications. Another static blending approach is presented in [14], where control inputs are allocated such that dominating modes can be controlled with a simplified control law. In case only a single mode needs to be controlled, according static decoupling approaches are proposed in [15] and [16]. While in [16], the input and output blending vectors are computed iteratively, [15] directly exploits the shape of the mode to be controlled. Apart from the direct blending for individual mode isolation, SISO controller designs may also be enabled by diagonalizing the whole underlying MIMO system such that each input controls a single output. Respective algorithms are well summarized and documented in [17].

Compared to the mentioned literature, the static blending approach proposed herein not only aims to decouple a single mode but also aims to maximize its controllability and observability in terms of the $\mathcal{H}_2$ norm. This allows for reducing the feedback gains of the SISO controller and thereby minimizes actuator action and increases robustness. The general idea of

M. Pusch is with the Department of System Dynamics and Control, German Aerospace Center (DLR), D-82234 Weßling, Germany (e-mail: manuel.pusch@dlr.de).

D. Ossmann is with the Department of Mechanical, Automotive and Aeronautical Engineering, Munich University of Applied Sciences, D-80335 Munich, Germany (e-mail: daniel.ossmann@hm.edu).

Manuscript received Mai 25, 2018; revised February 22, 2019.

the proposed blending approach for modal control is described in Section II. A numerically efficient algorithm for jointly computing the $\mathcal{H}_2$-optimal input and output blending vectors is derived in Section IV, based on the mathematical background given in Section III. Eventually, a numerical example is presented in Section V, where the proposed modal control approach is successfully applied to a simplified flexible aircraft model.

II. Modal Control

In this section, the concept of blending inputs and outputs for modal control is introduced. The proposed approach aims to control individual modes by means of simple SISO controllers independent of the number of inputs or outputs of the underlying dynamic system.

A. Modal Description of Linear Time-invariant Systems

A linear time-invariant (LTI) system with n_u inputs, n_y outputs and n_x states which is physically realizable can be described by the transfer function matrix

$$G(s) = C\left(sI - A\right)^{-1} B + D, \tag{1}$$

where $A \in \mathbb{R}^{n_x \times n_x}, B \in \mathbb{R}^{n_x \times n_u}, C \in \mathbb{R}^{n_y \times n_x}, D \in \mathbb{R}^{n_y \times n_u}$ and s denotes the Laplace variable. Assuming that A is diagonalizable, a modal decomposition of $G(s)$ is possible such that

$$G(s) = \sum_{i=1}^{n_i} M_i(s) + D,$$

where the individual modes $i = 1, ..., n_i$ are given as

$$M_i(s) = \begin{cases} \dfrac{R_i}{s - p_i} & \text{if } \Im(p_i) = 0 \\ \dfrac{R_i}{s - p_i} + \dfrac{\overline{R}_i}{s - \overline{p}_i} & \text{otherwise.} \end{cases} \tag{2}$$

According to Equation (2), a mode i is either described by a single real pole p_i with an imaginary part $\Im(p_i) = 0$ or a conjugate complex pole pair p_i and $\overline{p}_i$. Hence, the number of modes n_i does not necessarily equal the number of states n_x, i.e. $n_i \leq n_x$. Each pole p_i is associated with a residue $R_i = c_i b_i^T \in \mathbb{C}^{n_y \times n_u}$, where $b_i \in \mathbb{C}^{n_u}$ and $c_i \in \mathbb{C}^{n_y}$ are the pole input and output vectors, respectively. For a real pole, the corresponding pole vectors and residue are real, and for a conjugate complex pole pair the pole vectors and residues are conjugate complex.

In general, a mode i is considered to be asymptotically stable if $\Re(p_i) < 0$ and unstable if $\Re(p_i) > 0$. In case $\Re(p_i) = 0$, the mode is considered to be undamped, which also includes a pole in the origin. Furthermore, the natural frequency of a mode is given as $\omega_{\mathrm{n},i} = |p_i|$ and for $\omega_{\mathrm{n},i} \neq 0$, the corresponding relative damping is $\zeta_i = -\Re(p_i)/\omega_{\mathrm{n},i}$. Note that for a conjugate complex pole pair, the corresponding real parts $\Re(p_i) = \Re(\overline{p}_i)$ and magnitudes $|p_i| = |\overline{p}_i|$ are equal. For more information on modal decomposition and the properties of individual modes see, for instance, [5].

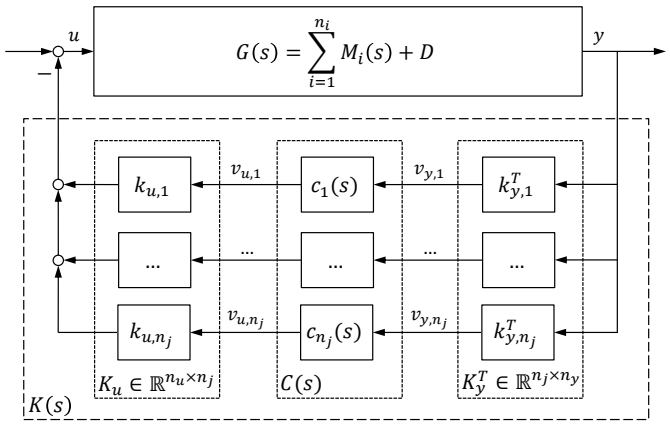

Fig. 1. Closed-loop interconnection of plant $G(s)$ with controller $K(s)$.

B. Modal Control using Blended Inputs and Outputs

The task of controlling a single mode $M_j(s) \in \{M_i(s)\}$, which is assumed to be well observable and controllable, can quickly become challenging when the number of control inputs or measurement outputs is increased. In order to reduce the complexity of the control problem, it is proposed to weight and sum up the measurement signals such that the resulting virtual measurement output $v_{y,j}$ represents the response of the mode to be controlled. Similarly, it is proposed to generate a virtual control input $v_{u,j}$ which is distributed to available control inputs such that the target mode can be individually controlled. In other words, the mode to be controlled is isolated (as good as possible) by blending inputs and outputs. The corresponding input and output blending vectors $k_{u,j} \in \mathbb{R}^{n_u}$ and $k_{y,j} \in \mathbb{R}^{n_y}$ depend on the shape of the targeted mode and can be seen as directional filters. This implies a high robustness against frequency variations as the blending vectors are independent of the mode's natural frequency. Blending the inputs and outputs as proposed, a simple SISO controller $c_j(s)$ can be designed to control the isolated mode. Hence, the MIMO control design problem becomes a SISO one with the challenge to find adequate blending vectors, which is the main focus of this article and described in detail in Section IV.

In Figure 1, the resulting feedback interconnection is depicted, where the modes $j = 1, .., n_j$ are subject to be controlled. Summarizing the input and output blending vectors in $K_u = \begin{bmatrix} k_{u,1} & \cdots & k_{u,n_j} \end{bmatrix}$ and $K_y = \begin{bmatrix} k_{y,1} & \cdots & k_{y,n_j} \end{bmatrix}$, the overall controller is

$$K(s) = K_u C(s) K_y^T,$$

where the SISO controllers are collected on the diagonal of $C(s) = \operatorname{diag}\left(c_1(s), \cdots, c_{n_j}(s)\right)$.

III. Mathematical Background

The blending vector design problem considered in this article can be formulated as a constrained nonlinear optimization problem. In order to allow for a numerically efficient solution of this optimization problem, it is reformulated by means of the mathematical formulas given in this section.

A. $\mathcal{H}_2$ Norm

In this article, the $\mathcal{H}_2$ norm is used as an objective function for designing the blending vectors to individually control the modes $M_j(s)$. Blending the inputs and outputs of $M_j(s)$, a SISO system of first or second order is derived, for which the $\mathcal{H}_2$ norm can be computed in a very efficient way as given here.

Definition 1 ([5])**.** *The $\mathcal{H}_2$ norm of an asymptotically stable and strictly proper LTI system $G(s)$ can be defined as*

$$\|G(s)\|_{\mathcal{H}_2} = \sqrt{\frac{1}{2\pi}\int_{-\infty}^{\infty} \mathrm{Tr}\left[G(j\omega)^H G(j\omega)\right] d\omega}, \tag{3}$$

where j denotes the imaginary unit defined by its property $j^2 = -1$.

In general, the $\mathcal{H}_2$ norm of a given LTI system is computed by solving a Lyapunov equation, see [18] for more details. For first or second order SISO systems, however, an alternative way for computing the $\mathcal{H}_2$ norm is derived, which is fundamental for the proposed blending vector design.

Lemma 1 ($\mathcal{H}_2$ norm of first or second order SISO system)**.** *Let the transfer function $g(s) : \mathbb{C} \to \mathbb{C}$ be given and describe a strictly proper and asymptotically stable LTI system with a maximum order of two. Furthermore, let ω_n and ζ denote the natural frequency and relative damping of $g(s)$. Then,*

$$\|g(s)\|_{\mathcal{H}_2} = |g(j\omega_\mathrm{n})| \sqrt{\omega_\mathrm{n}\zeta}. \tag{4}$$

Proof. The proof is shown for an LTI system with a single conjugate complex pole pair. For a system with real-valued poles, the proof may be derived the same way and is not described here.

To begin with, a state space representation for

$$g(s) = \frac{r}{s-p} + \frac{\overline{r}}{s-\overline{p}} = C\left(sI - A\right)^{-1} B + D$$

is chosen as

$$A = \begin{bmatrix} -p & 0 \\ 0 & -\overline{p} \end{bmatrix}, B = \begin{bmatrix} 1 \\ 1 \end{bmatrix}, C = \begin{bmatrix} r & \overline{r} \end{bmatrix}, D = 0,$$

where r and $\overline{r}$ denote the conjugate complex (scalar) residues associated to the conjugate complex pole pair p and $\overline{p}$. By analytically solving the Lyapunov equation

$$AW_c + W_c A^H + BB^H = 0,$$

the controllability Gramian matrix can then be computed as

$$W_\mathrm{c} = -\begin{bmatrix} \frac{1}{p+\overline{p}} & \frac{1}{2p} \\ \frac{1}{2\overline{p}} & \frac{1}{p+\overline{p}} \end{bmatrix}.$$

According to [18], the squared $\mathcal{H}_2$ norm can then be computed as

$$\begin{aligned} \|g(s)\|_{\mathcal{H}_2}^2 &= CW_\mathrm{c}C^H \\ &= -\frac{4p\overline{p}r\overline{r} + (r^2\overline{p} + \overline{r}^2 p)(p+\overline{p})}{2p\overline{p}(p+\overline{p})}. \end{aligned} \tag{5}$$

Similarly, an analytic computation of the squared right hand side of Equation (4) results in

$$\begin{aligned} |g(j\omega_\mathrm{n})|^2 \omega_\mathrm{n}\zeta &= -\frac{1}{2}(p+\overline{p})\left|g\left(j\sqrt{p\overline{p}}\right)\right|^2 \\ &= -\frac{4p\overline{p}r\overline{r} + (r^2\overline{p} + \overline{r}^2 p)(p+\overline{p})}{2p\overline{p}(p+\overline{p})}, \end{aligned}$$

which obviously equals the result of Equation (5). □

Remark 1. *The natural frequency ω_n and relative damping ζ for a system with a single real pole or a conjugate complex pole pair are defined in Section III-C. For a system with two real-valued poles $p_1 < 0$ and $p_2 < 0$, $\omega_\mathrm{n} = \sqrt{p_1 p_2}$ and $\zeta = -\frac{p_1+p_2}{2\omega_n}$.*

B. Euclidean Norm of a Complex Number

Computing the $\mathcal{H}_2$ norm according to Lemma 1 requires to compute the absolute value of a complex number, also known as its Euclidean norm. In this article, a rather uncommon way of computing the Euclidean norm is used, which is defined as follows.

Definition 2 (Euclidean norm of a complex number)**.** *Let $w \in \mathbb{C}$ be given and the corresponding real and imaginary part be denoted as $\Re(w)$ and $\Im(w)$, respectively. Then,*

$$|w| = \max_{\phi\in\mathbb{R}} \left(\Re(w)\cos\phi + \Im(w)\sin\phi\right).$$

The intuition behind this definition is that the Euclidean norm of a complex number can be directly read by rotating it onto the positive real axis in the complex plane.

C. LTI System Decomposition

In this section, a decomposition for LTI systems is described which allows for a reduction of the computational cost of the presented blending vector design algorithm.

Lemma 2 (LTI system decomposition)**.** *Let the strictly proper and physically realizable LTI system $G(s)$ of order n_x be given and have n_u inputs and n_y outputs. Then, there exists a decomposition*

$$G(s) = Q_C \tilde{G}(s) Q_B^T, \tag{6}$$

where $\tilde{G}(s)$ describes a strictly proper LTI system of order n_x with $n_{\tilde{u}} \leq n_x$ inputs and $n_{\tilde{y}} \leq n_x$ outputs, and both $Q_C \in \mathbb{R}^{n_y \times n_{\tilde{y}}}$ and $Q_B \in \mathbb{R}^{n_u \times n_{\tilde{u}}}$ form an orthonormal basis, respectively.

Proof. According to Equation (1), a strictly proper transfer function matrix is given by

$$G(s) = C\left(sI - A\right)^{-1} B,$$

where the feedthrough matrix $D = 0$. Carrying out a thin QR decomposition on

$$\begin{aligned} B^T &= Q_B R_B \text{ and} \\ C &= Q_C R_C \end{aligned}$$

it can be written

$$\tilde{G}(s) = R_C\left(sI - A\right)^{-1} R_B^T,$$

where $R_B \in \mathbb{R}^{n_{\bar{u}} \times n_{\bar{u}}}$, $R_C \in \mathbb{R}^{n_{\bar{y}} \times n_{\bar{y}}}$, and both $Q_B \in \mathbb{R}^{n_u \times n_{\bar{u}}}$ and $Q_C \in \mathbb{R}^{n_y \times n_{\bar{y}}}$ form an orthonormal basis, respectively. □

IV. $\mathcal{H}_2$-optimal Blending of Inputs and Outputs

In this section, the blending vector design problem is derived and a numerically efficient solution is provided. The goal addressed herein is to find blending vectors which yield a maximum modal controllability and observability in terms of the $\mathcal{H}_2$ norm. This requires a joint design of the input and output blending vectors as controllability and observability can not be regarded independent of each other. Furthermore, a sufficient mode decoupling needs to be considered in order to enable the proposed SISO controller design. Eventually, the proposed method is extended to undamped and unstable modes, for which the $\mathcal{H}_2$ norm becomes infinite by definition.

A. Maximization of Modal Controllability and Observability

The combined controllability and observability of an asymptotically stable mode $M(s) \in \{M_j(s)\}$ is quantified in terms of the $\mathcal{H}_2$ norm. Hence, the goal is to stay as close as possible to the original controllability and observability of the targeted mode when blending inputs and outputs with real-valued unit vectors k_u and k_y, respectively. This gives rise to quantify the loss of controllability and observability via the efficiency factor

$$\eta = \frac{\left\| k_y^T M(s) k_u \right\|_{\mathcal{H}_2}}{\left\| M(s) \right\|_{\mathcal{H}_2}}, \tag{7}$$

where $\eta \in [0\ 1]$ for $M(s)$ being controllable and observable. Based on that, a pair of input and output blending vectors is considered as $\mathcal{H}_2$-optimal when the efficiency factor η is maximized. The resulting optimization problem can hence be formulated as

$$\begin{aligned} \underset{k_u \in \mathbb{R}^{n_u}, k_y \in \mathbb{R}^{n_y}}{\text{maximize}} \quad & \left\| k_y^T M(s) k_u \right\|_{\mathcal{H}_2} \\ \text{subject to} \quad & \left\| k_u \right\|_2 = 1 \\ & \left\| k_y \right\|_2 = 1. \end{aligned} \tag{8}$$

In order to efficiently solve the nonlinear optimization problem (8), Lemma 1 is applied to the objective function of (8) giving

$$\left\| k_y^T M(s) k_u \right\|_{\mathcal{H}_2} = |k_y^T M(j\omega_\mathrm{n}) k_u| \sqrt{\omega_\mathrm{n} \zeta}, \tag{9}$$

where the term $\sqrt{\zeta \omega_\mathrm{n}}$ is actually independent of the blending vectors. Hence, the original problem of maximizing the $\mathcal{H}_2$ norm in (8) can be turned into a problem of maximizing the magnitude of the complex scalar $k_y^T M(j\omega_\mathrm{n}) k_u$. Computing this magnitude according to Definition 2 and factoring out the real-valued blending vectors k_y and k_u, it can be written

$$|k_y^T M(j\omega_\mathrm{n}) k_u| = \max_{\phi} \left(k_y^T F(\phi) k_u \right), \tag{10}$$

where $F(\phi) : \mathbb{R} \to \mathbb{R}^{n_y \times n_u}$ is defined as

$$F(\phi) = \Re(M(j\omega_\mathrm{n})) \cos\phi + \Im(M(j\omega_\mathrm{n})) \sin\phi. \tag{11}$$

Recalling that the actual goal is to find a maximum of Equation (10) gives

$$\begin{aligned} \max_{k_u, k_y} \left| k_y^T M(j\omega_\mathrm{n}) k_u \right| &= \max_{k_u, k_y} \max_{\phi} \left(k_y^T F(\phi) k_u \right) \\ &= \max_{\phi} \max_{k_u, k_y} \left(k_y^T F(\phi) k_u \right). \end{aligned} \tag{12}$$

In Equation (12), the term

$$\max_{k_u, k_y} \left(k_y^T F(\phi) k_u \right) = \left\| F(\phi) \right\|_2 = \sigma_\mathrm{max} \tag{13}$$

can be directly computed for a given value of ϕ by applying a singular value decomposition (SVD) on

$$\begin{aligned} F(\phi) &= U \Sigma V^T \\ &= \begin{bmatrix} k_{y,\mathrm{max}} & \bullet \end{bmatrix} \begin{bmatrix} \sigma_\mathrm{max} & 0 \\ 0 & \bullet \end{bmatrix} \begin{bmatrix} k_{u,\mathrm{max}} & \bullet \end{bmatrix}^T, \end{aligned} \tag{14}$$

where the placeholder $\bullet$ denotes a matrix of adequate size. In Equation (14), both $U \in \mathbb{R}^{n_y \times n_y}$ and $V \in \mathbb{R}^{n_u \times n_u}$ are orthogonal matrices which are real-valued as $F(\phi)$ is also real-valued. Furthermore, $\Sigma \in \mathbb{R}^{n_y \times n_u}$ is a rectangular diagonal matrix with the singular values of $F(\phi)$ in descending order on its diagonal. Selecting only the largest singular value $\sigma_\mathrm{max} \in \mathbb{R}_{\geq 0}$, the corresponding input and output singular vectors $k_{u,\mathrm{max}} \in \mathbb{R}^{n_u}$ and $k_{y,\mathrm{max}} \in \mathbb{R}^{n_y}$ directly yield the input and output blending vectors which solve Equation (13) for a given value of ϕ.

Finally, inserting Equation (13) into Equation (12), an equivalent formulation of the optimization problem (8) is given as

$$\max_{k_u, k_y} \left\| k_y^T M(s) k_u \right\|_{\mathcal{H}_2} \Leftrightarrow \max_{\phi} \left\| F(\phi) \right\|_2, \tag{15}$$

where the optimization variables $k_u \in \mathbb{R}^{n_u}$ and $k_y \in \mathbb{R}^{n_y}$ are constrained by $\left\| k_u \right\|_2 = 1$ and $\left\| k_y \right\|_2 = 1$ while $\phi \in \mathbb{R}$ is unconstrained. Solving $\max_\phi \left\| F(\phi) \right\|_2$ yields an optimal phase angle ϕ^* for which the $\mathcal{H}_2$-optimal blending vectors can be directly determined according to Equation (14). Hence, the number of optimization variables is reduced from $n_u + n_y$ to a single one, or, in other words, the difficulty of finding a solution of (8) becomes independent of the actual number of inputs and outputs.

B. Mode Decoupling

So far, $\mathcal{H}_2$-optimal blending vectors are derived which maximize the controllability and observability of the targeted mode. However, the residual modes may still be controlled or measured by the blended inputs and outputs, which is commonly known as spillover. To avoid spillover, the target mode needs to be decoupled. This can be achieved by considering dynamic filters as notch or band-stop filters in SISO controller design, where the target and residual modes need to be well separated in frequency. If this is not the case, it is proposed to exploit the shape of the respective residual modes and enforce the input and output blending vectors to be orthogonal on them, or more specifically on its pole input and output vectors described in Section II-A. For a complex-valued pole vector, this means that orthogonality is enforced on both the real and imaginary part. Collecting the real and imaginary parts of the

respective pole input and output vectors as row vectors in the matrices P_u and P_y, the original optimization problem (8) can be augmented as

$$\begin{array}{ll} \underset{k_u\in\mathbb{R}^{n_u},k_y\in\mathbb{R}^{n_y}}{\text{maximize}} & \left\|k_y^T M(s) k_u\right\|_{\mathcal{H}_2} \\ \text{subject to} & \|k_u\|_2 = 1 \\ & \|k_y\|_2 = 1 \\ & P_u k_u = 0 \\ & P_y k_y = 0, \end{array} \tag{16}$$

where the constraints $P_u k_u = 0$ and $P_y k_y = 0$ enforce the desired mode decoupling. For the blending vectors k_u and k_y, this means that they are restricted to the null space of P_u and P_y, respectively. If one of the null spaces is empty, meaning that P_u or P_y has full rank, the augmented optimization problem (16) is infeasible. This also implies that for a finite number of inputs and outputs, the number of residual modes which can be made uncontrollable or unobservable is limited. Note, however, that for mode decoupling it may be sufficient to make the respective residual modes either uncontrollable or unobservable but not both.

In order to solve the augmented optimization problem (16), the original optimization variables k_u and k_y are substituted by

$$k_u = N_u \hat{k}_u \tag{17}$$

$$k_y = N_y \hat{k}_y \ , \tag{18}$$

where N_u and N_y denote an orthonormal basis of the null space of P_u and P_y, respectively. With the vectors $\hat{k}_u$ and $\hat{k}_y$ as new optimization variables, the equivalent optimization problem (15) can be turned into

$$\max_{\hat{k}_u,\hat{k}_y} \left\|\hat{k}_y^T N_y^T M(s) N_u \hat{k}_u\right\|_{\mathcal{H}_2} \ \Leftrightarrow \ \max_{\phi} \left\|N_y^T F(\phi) N_u\right\|_2, \tag{19}$$

since the real-valued matrices N_u and N_y act as unitary linear transformations preserving the inner product. This means that iff $\hat{k}_u$ and $\hat{k}_y$ are real-valued unit vectors, k_u and k_y are also real-valued unit vectors. Solving the equivalent optimization problem (19) for ϕ, solutions for $\hat{k}_u$ and $\hat{k}_y$ can be determined by the SVD in Equation (14) which yield the $\mathcal{H}_2$-optimal blending vectors when multiplied with N_u and N_y, respectively.

It should be noted that the additional mode decoupling constraints typically decrease the maximum achievable $\mathcal{H}_2$ norm. Hence, a trade-off between the decoupling of individual modes and the attainable controllability and observability of the mode to be controlled is usually required.

Furthermore, the described procedure for mode decoupling can also be used to eliminate a non-zero feedthrough matrix $D \neq 0$. For this purpose, the right or left singular vectors of D need to be added to P_u or P_y, respectively.

C. Computational Aspects

Considering the original optimization problem (8), its solution according to Equation (15) requires to carry out an SVD on $F(\phi)$ for each iteration of ϕ. The computational cost of a single SVD largely depends on the size of $F(\phi)$, which is given by the number of inputs and outputs of the underlying system $G(s)$. Hence, if $G(s)$ has a large number of inputs and outputs, the computational effort to solve (15) may be high and lack of numerical accuracy. For this reason, it is suggested to previously decompose $M(s)$ according to Lemma 2. In case also mode decoupling is enforced, the matrices N_u and N_y given in Section IV-B are multiplied first and then the proposed decomposition is carried out resulting in

$$N_y^T M(s) N_u = Q_C \tilde{M}(s) Q_B^T. \tag{20}$$

In Equation (20), $\tilde{M}(s)$ has $n_{\tilde{u}} \leq 2$ inputs and $n_{\tilde{y}} \leq 2$ outputs as a minimal realization of $M(s)$ has a maximum order of two. Knowing that both Q_B and Q_C form a real-valued orthonormal basis, $\left\|N_y^T M(s) N_u\right\|_2 = \left\|\tilde{M}(s)\right\|_2$ holds. This allows reformulating Equation (19) as

$$\max_{\hat{k}_u,\hat{k}_y} \left\|\hat{k}_y^T N_y^T M(s) N_u \hat{k}_u\right\|_{\mathcal{H}_2} \ \Leftrightarrow \ \max_{\phi} \left\|\tilde{F}(\phi)\right\|_2, \tag{21}$$

where $\tilde{F}(\phi) : \mathbb{R} \to \mathbb{R}^{n_{\tilde{y}} \times n_{\tilde{u}}}$ is defined as

$$\tilde{F}(\phi) = \Re(\tilde{M}(j\omega_\mathrm{n})) \cos\phi + \Im(\tilde{M}(j\omega_\mathrm{n})) \sin\phi. \tag{22}$$

As the matrix returned by $\tilde{F}(\phi)$ has a maximum size of 2×2, the term $\left\|\tilde{F}(\phi)\right\|_2$ and also its derivative $\partial \left\|\tilde{F}(\phi)\right\|_2 / \partial\phi$ can be computed analytically as given, for instance, in [5]. For optimization, this means that computational effort and numerical inaccuracy can be greatly reduced, especially when the given number of inputs and outputs is high.

Note that if the real or imaginary part of $M(j\omega_\mathrm{n})$ is zero, the $\mathcal{H}_2$-optimal blending vectors can be computed without the need of solving optimization problem (19), which makes the proposed decomposition unnecessary for this special case.

D. Summary of the Proposed Algorithm

Summing up the findings of Sections IV-A to IV-C, the optimization problem with included mode decoupling constraints (16) can be efficiently solved by first finding an optimal phase angle

$$\phi^* = \arg\max_{\phi\in\mathbb{R}} \left\|\tilde{F}(\phi)\right\|_2, \tag{23}$$

where $\tilde{F}(\phi)$ is defined in Equation (22). Due to the given periodicity of $\tilde{F}(\phi)$, the search for an optimal phase angle may be restricted to an interval of size π, for instance $\phi \in [0, \pi[$.

After determining the optimal phase angle ϕ^*, the corresponding $\mathcal{H}_2$-optimal input and output blending vectors $k_u^* = N_u Q_B \tilde{k}_u^*$ and $k_y^* = N_y Q_C \tilde{k}_y^*$ can be derived by means of an SVD of

$$\tilde{F}(\phi^*) = U \Sigma V^T = \begin{bmatrix} \tilde{k}_y^* & \bullet \end{bmatrix} \begin{bmatrix} \sigma_{\max}^* & 0 \\ 0 & \bullet \end{bmatrix} \begin{bmatrix} \tilde{k}_u^* & \bullet \end{bmatrix}^T, \tag{24}$$

where $\sigma_{\max}^* = \left\|\tilde{F}(\phi^*)\right\|_2 = \left\|N_y^T F(\phi) N_u\right\|_2$ is the optimal value of the objective function in Equation (23). Note that the optimal phase angle and the resulting optimal blending vectors are not necessarily unique. This can be shown at the example of the real and imaginary part of $M(j\omega_\mathrm{n})$ having equal singular values but orthogonal singular vectors.

E. Undamped and Unstable Modes

Undamped Modes: According to Section II, a mode $M(s)$ with a real pole p or a conjugate complex pole pair p and $\overline{p}$ is considered undamped if $\Re(p) = 0$. While the corresponding $\mathcal{H}_2$ norm becomes infinite in this case, a finite limit for the efficiency factor η defined in Equation (7) can be computed as

$$\lim_{\Re(p)\to 0^-} \eta = \lim_{\Re(p)\to 0^-} \frac{\left\|k_y^T M(s) k_u\right\|_{\mathcal{H}_2}}{\|M(s)\|_{\mathcal{H}_2}} = \frac{\left\|k_y^T R k_u\right\|_2}{\|R\|_2},$$

where R denotes the residue associated to pole p. Based on that, the matrix function $F(\phi)$ defined in Equation (11) can be replaced by

$$F_{\lim}(\phi) = \Re(R)\cos\phi + \Im(R)\sin\phi.$$

Equally, the matrix function $\tilde{F}(\phi)$ defined in Equation (22) can be replaced by

$$\tilde{F}_{\lim}(\phi) = \Re(\tilde{R})\cos\phi + \Im(\tilde{R})\sin\phi,$$

where $\tilde{R}$ denotes the residue of $\tilde{M}(s)$ from Equation (20). The $\mathcal{H}_2$-optimal blending vectors can then be derived by first computing $\phi^* = \arg\max_\phi \left\|\tilde{F}_{\lim}(\phi)\right\|_2$ and subsequently computing the singular vectors of $\tilde{F}_{\lim}(\phi^*)$, see Section IV-D for more details.

Unstable Modes: Similarly to an undamped mode, the $\mathcal{H}_2$ norm of an unstable mode with $\Re(p) > 0$ is also infinite. Taking Definition 1, which describes the $\mathcal{H}_2$ norm of an asymptotically stable system, it can be seen that the $\mathcal{H}_2$ norm becomes a maximum iff the integral over the (squared) magnitude of the frequency response becomes a maximum. For an unstable mode, this integral can also be computed by exploiting the fact that the magnitude is not affected when mirroring the unstable pole(s) across the imaginary axis. As a result, an asymptotically stable system is obtained for which the $\mathcal{H}_2$ norm can be computed as given in Section III-A. Based on that, it is proposed to design the blending vectors of an unstable mode by first mirroring the underlying poles across the imaginary axis and then applying the algorithm described above. Note that in order to preserve the magnitude of the frequency response when mirroring a pole, the zeros of each individual transfer channel need to be preserved which typically affects the corresponding residue(s).

V. Numerical Example

To demonstrate the effectiveness of the proposed control approach, it is applied to a flexible aircraft with lightly damped modes. For replicability reasons, a low-order approximation of the high-order aeroelastic model is used in this article. Thereby, the numerical values of the model as well as the resulting controller can be provided herein. For realistic physical applications, the reader is referred to [19], [20] and [21], where the proposed blending approach is successfully applied to different aeroelastic systems.

A. System Description

The example given in this article is based on an aeroelastic model of a large transport aircraft with distributed flaps and measurements taken from [19]. The model used represents only the three most dominating modes, where the corresponding properties are summarized in Table I. The underlying state space matrices are provided in the Appendix, with the system featuring four control inputs and eight measurement outputs. The four control inputs represent symmetric deflections commands for three pairs of trailing edge flaps on the wing and one pair of elevators. The measurement outputs are four vertical acceleration and four rotational rate sensors placed on the wings of the aircraft.

TABLE I
Modes $M_i(s)$ in the Frequency Range of Interest.

i	natural frequency $\omega_{\mathrm{n},i}$	relative damping ζ_i
1	1.6 rad/s	0.42
2	10.9 rad/s	0.12
3	18.4 rad/s	0.03

B. Blending of Inputs and Outputs

In order to reduce structural loads of the aircraft, the control objective herein is to increase the damping of mode 2 and 3. To that end, the inputs and outputs of the underlying system are blended aiming to isolate both modes. For comparison reasons, the blending vector design is carried out with and without explicit mode decoupling constraints.

In a first step, blending vectors are designed to maximize controllability and observability of the two modes without considering any mode decoupling constraints. The resulting optimization problem is described in Equation (8) and solved according to Equation (15). In Figure 2, the resulting efficiency factor $\eta(\phi) = \sqrt{\omega_\mathrm{n}\zeta}\,\|F(\phi)\|_2/\|M(s)\|_{\mathcal{H}_2}$ as a function of the optimization variable ϕ is plotted for mode 2 (——) and mode 3 (·····). It can be seen that the respective maxima can easily be found using some gradient-based optimization algorithm. Blending the inputs and outputs with the obtained blending vectors results in a system with two virtual control inputs and two virtual control outputs. In Figure 3, the magnitudes of the corresponding transfer functions are plotted, where it has to be acknowledged that the individual modes are still coupled.

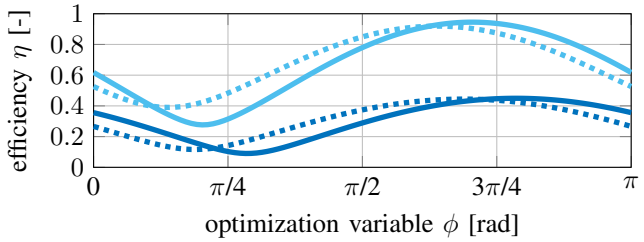

Fig. 2. Comparison of efficiency factor η with (——, ·····) and without (——, ·····) mode decoupling constraints for mode 2 (solid lines) and mode 3 (dashed lines).

Hence, in a second step, blending vectors are designed taking into account also mode decoupling constraints. In order to leave mode 1 unaffected, it needs to be either uncontrollable

by the blended inputs or unobservable by the blended outputs. For the latter, the maximum achievable efficiency factor η is considerably larger because the number of measurement outputs is much larger than the number of control inputs. Thus, mode 1 is only made unobservable by enforcing the output blending vectors $k_{y,2}$ and $k_{y,3}$ to be orthogonal on its pole output vector c_1. In other words, an explicit decoupling from mode 1 is achieved with the constraints $c_1^T k_{y,2} = 0$ and $c_1^T k_{y,3} = 0$. Additionally, an independent control of mode 2 and mode 3 is desired. This can be achieved by enforcing the input and output blending vectors of one mode to be orthogonal on the pole input and output vectors of the other mode. The corresponding constraints for input blending are $b_3^T k_{u,2} = 0$ and $b_2^T k_{u,3} = 0$, where b_2 and b_3 are the pole input vectors of mode 2 and mode 3, respectively. Similarly, the output blending vectors are constrained by $c_3^T k_{y,2} = 0$ and $c_2^T k_{y,3} = 0$ with c_2 and c_3 denoting the respective pole output vectors. Solving the augmented optimization problem (16) by means of Equation (19), the $\mathcal{H}_2$-optimal blending vectors are computed according to Equation (24) as

$$K_u = \begin{bmatrix} -0.06 & -0.56 \\ -0.48 & -0.03 \\ -0.85 & 0.67 \\ 0.19 & 0.49 \end{bmatrix} \text{ and } K_y = \begin{bmatrix} 0.43 & 0.38 \\ 0.06 & -0.62 \\ -0.43 & -0.17 \\ -0.54 & 0.42 \\ 0.50 & 0.40 \\ 0.21 & -0.30 \\ -0.18 & -0.15 \\ 0.082 & 0.012 \end{bmatrix}.$$

The successful decoupling of modes can be seen in Figure 3, where the modes to be controlled are clearly emphasized in the respective channels while no other modes are visible. It needs to be mentioned, however, that the enforced mode decoupling leads to a degradation of the maximum achievable efficiency factor η as it is recognizable in Figure 2. This can also be seen in Figure 3, where the resonance peaks of the target modes are reduced when considering mode decoupling. Taken as a whole, this trade-off is acceptable as sufficient controllability and observability of the target modes are still given.

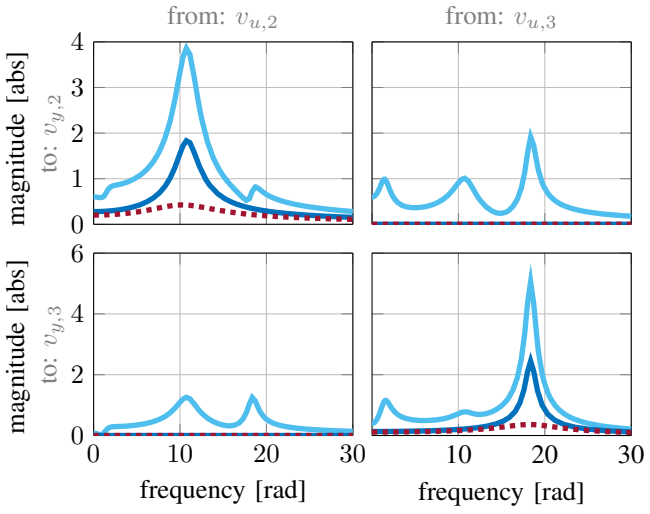

Fig. 3. Comparison of frequency response from blended inputs to blended outputs with (—) and without (—) mode decoupling constraints together with the closed-loop response (····).

C. SISO Controller Design

In the ideal case the input and output blending fully decouples a conjugate complex mode $M(s)$ from its parent system $G(s)$, it holds

$$k_y^T G(s) k_u = k_y^T M(s) k_u = \frac{\alpha s + \beta}{s^2 + 2\zeta\omega_\mathrm{n} s + \omega_\mathrm{n}^2}. \tag{25}$$

In Equation (25), ω_n and ζ denote the natural frequency and relative damping of the decoupled mode. Furthermore, the coefficients $\alpha \in \mathbb{R}$ and $\beta \in \mathbb{R}$ result from blending inputs and outputs with the vectors k_u and k_y, respectively. In order to increase the damping of the decoupled mode (25), a SISO feedback controller needs to be designed. In general, the relative damping of a mode can be increased by a so-called direct velocity feedback, see [6]. For the decoupled mode (25), this can be achieved by filtering the blended output signal with

$$h(s) = \begin{cases} 1/\alpha & \text{if } \beta = 0 \\ s/\beta & \text{if } \alpha = 0 \\ \operatorname{sgn}(\alpha)(s + \alpha\omega_\mathrm{n}^2/\beta) & \text{otherwise.} \end{cases}$$

In case $\beta = 0$, modal velocity is already measured by the blended output and hence, a proportional feedback directly allows increasing relative damping. In case $\alpha = 0$, the blended output represents modal deflection, which needs to be differentiated in order to obtain a velocity signal. In any other case, the proposed proportional-derivative (PD) controller adds a zero $z = -\alpha\omega_\mathrm{n}^2/\beta$ such that a static feedback of the resulting signal directly affects the relative damping of the target mode. To suppress high-frequency amplification, the derivative term is commonly approximated as $s \approx s/(Ts+1)$, where $T \in \mathbb{R}^+$ denotes the time constant of the added low-pass filter. If the target mode can not be fully decoupled, which is generally the case, the SISO controller may also include a dynamic filter $w(s)$ to emphasize or suppress certain frequencies. For instance, the bandwidth of the SISO controller may be restricted to the approximate frequency range of the target mode by band-pass filtering blended measurements accordingly. The resulting SISO controller is given as

$$c(s) = \lambda h(s) w(s),$$

where the static feedback gain $\lambda \in \mathbb{R}$ is subject to tuning. This additional degree of freedom allows to adjust control performance such that common constraints like actuator limitations or robustness criteria are met.

In the example given here, $T = 0.01$, $w(s) = 1$ and $\lambda = 0.1$ are chosen for both modes to be controlled. The resulting SISO controllers are hence $c_2(s) = -0.1\,(s/(0.01s+1) + 13.7)$ and $c_3(s) = -0.1\,(s/(0.01s+1) + 12.4)$, which are nothing but two phase-lead compensators. Closing the control loop in the presented example shifts the poles as given in Figure 4. It can be seen that the relative damping is increased by a factor of 3.2 and 5.9 for mode 2 and mode 3, respectively. On the contrary, mode 1 is not affected as an invariant zero is placed at its pole location when considering an explicit mode decoupling. Furthermore, the increased modal damping is also visible in Figure 3, where the resonance peaks are clearly reduced. Note that Figure 3 also allows a qualitative evaluation

of the energy absorbed by the (damped) modes considering the energy interpretations of the $\mathcal{H}_2$ and $\mathcal{H}_\infty$ norm [5].

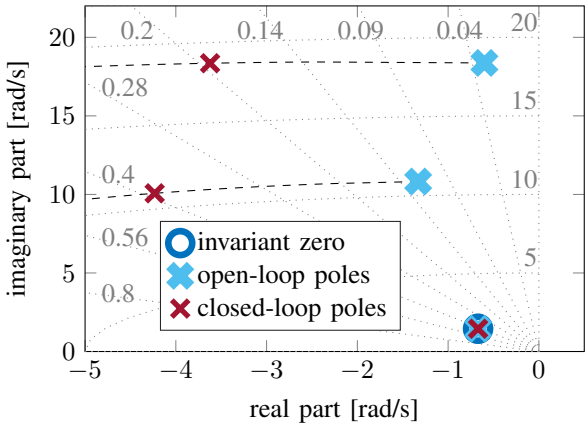

Fig. 4. Poles and invariant zero of the open- and closed-loop system with blended inputs and outputs together with the root locus illustration (- - -).

Reducing the number of actuators and sensors in general reduces (modal) controllability and observability and hence also the maximum achievable efficiency factor η^*. This, in turn, means that the feedback gain λ needs to be increased to yield an equal controller performance, which typically has adverse effects on robustness and control effort. For instance, using only the first five measurements in the given example reduces $\eta_2^* = 0.45$ to 0.32 and $\eta_3^* = 0.44$ to 0.16. Consequently, to maintain the closed-loop poles, the feedback gains λ for mode 2 and mode 3 need to be increased from 0.1 to 0.14 and 0.25, respectively. Note that in case the number of measurements is further reduced, the proposed mode decoupling is not possible anymore and a more advanced SISO controller design may be required.

VI. Conclusion

In this article, a novel modal control approach is presented for systems with a large number of control inputs and measurement outputs. The approach splits the challenge of designing a suitable MIMO controller into the blending of inputs and outputs and a subsequent SISO controller design. The goal for designing the corresponding blending vectors is to isolate the modes of interest and maximize their observability and controllability in terms of the $\mathcal{H}_2$ norm. A numerically efficient algorithm is derived which allows a joint computation of the interdependent input and output blending vectors by solving an unconstrained optimization problem in a single variable. The successful application of the proposed control approach to an aeroelastic system proves its effectiveness, where two modes are actively damped with first-order SISO controllers.

References

[1] M. Kraft and N. White, *MEMS for Automotive and Aerospace Applications*. Cambridge, UK: Woodhead Publishing, 01 2013.
[2] V. G. M. Annamdas, "Review on developments in fiber optical sensors and applications," *International Journal of Materials Engineering*, vol. 1, no. 1, pp. 1–16, 2011.
[3] S. Barbarino, O. Bilgen, R. M. Ajaj, M. I. Friswell, and D. J. Inman, "A review of morphing aircraft," *Journal of intelligent material systems and structures*, vol. 22, no. 9, pp. 823–877, 2011.
[4] N. Nguyen, "Elastically shaped future air vehicle concept," *NASA Innovation Fund Award*, 2010.
[5] S. Skogestad and I. Postlethwaite, *Multivariable feedback control: analysis and design*. Wiley New York, 2007, vol. 2.
[6] A. Preumont, *Vibration control of active structures*. Springer, 1997.
[7] L. Meirovitch and H. Baruh, "On the problem of observation spillover in self-adjoint distributed-parameter systems," *Journal of Optimization Theory and Applications*, vol. 39, no. 2, 1983.
[8] M. Balas, "Feedback control of flexible systems," *IEEE Transactions on Automatic Control*, pp. 673–679, 1978.
[9] M. F. Enzinger, "A modal control approach based on a minimum order dynamic feedback," Ph.D. dissertation, University of Hagen, 2007.
[10] S. Chughtai, A.Nobakhti, and H. Wang, "A systematic approach to the design of robust diagonal dominance based MIMO controllers," in *Proc. of 44th IEEE Conference on Decision and Control*, Sevilla, Spain, 2005.
[11] D. Inman, "Modal decoupling conditions for distributed control of flexible structures," *Journal of Guidance, Control, and Dynamics*, vol. 7, no. 6, pp. 750–752, 1984.
[12] M. Friswell, "On the design of modal actuators and sensors," *Journal of Sound and Vibration*, vol. 241, no. 3, pp. 361–372, 2001.
[13] M. Schneiders, M. Van De Molengraft, and M. Steinbuch, "Benefits of over-actuation in motion systems," in *Proc. of American Control Conference*, Boston, MA, USA, 2004, pp. 505–510.
[14] M. Pusch, "Allocation of distributed flaps for gust load alleviation," in *Proc. of 1st IEEE Conference on Control Technology and Applications*, Kohala Coast, HI, USA, 2017, pp. 2120–2125.
[15] R. Hoogendijk, M. H. M. van de Molengraft, and M. Steinbuch, "Directional notch filters for motion control of flexible structures," *Mechatronics*, vol. 24, no. 6, pp. 632–639, 2014.
[16] B. Danowsky, P. Thompson, D.-C. Lee, and M. Brenner, "Modal isolation and damping for adaptive aeroservoelastic suppression," in *AIAA Atmospheric Flight Mechanics Conference*, Boston, USA, 2013.
[17] D. Vaes, "Optimal static decoupling for multivariable control design," Ph.D. dissertation, University of Leuven, 2005.
[18] K. Zhou, J. C. Doyle, K. Glover *et al.*, *Robust and optimal control*. Prentice hall New Jersey, 1996, vol. 40.
[19] M. Pusch, "Aeroelastic mode control using $\mathcal{H}_2$-optimal blends for inputs and outputs," in *AIAA Guidance, Navigation, and Control Conference*, Orlando, FL, USA, 2018.
[20] M. Pusch, D. Ossmann, J. Dillinger, T. M. Kier, M. Tang, and J. Lübker, "Aeroelastic modeling and control of an experimental flexible wing," in *AIAA Guidance, Navigation, and Control Conf.*, San Diego, USA, 2019.
[21] T. Luspay, T. Baár, D. Teubl, B. Vanek, D. Ossmann, M. Wüstenhagen, M. Pusch, T. M. Kier, S. Waitman, A. Ianelli, A. Marcos, and M. Lowenberg, "Flight control design for a highly flexible flutter demonstrator," in *AIAA Atmospheric Flight Mechanics Conf.*, San Diego, USA, 2019.

Appendix

The state space matrices of the numerical example used in Section V are given in a real Jordan normal form as

$$A = \begin{bmatrix} -0.67 & -1.45 & 0 & 0 & 0 & 0 \\ 1.45 & -0.67 & 0 & 0 & 0 & 0 \\ 0 & 0 & -1.33 & -10.82 & 0 & 0 \\ 0 & 0 & 10.82 & -1.33 & 0 & 0 \\ 0 & 0 & 0 & 0 & -0.6 & -18.37 \\ 0 & 0 & 0 & 0 & 18.37 & -0.6 \end{bmatrix}$$

$$B = \begin{bmatrix} 0.01 & -0.01 & -0.01 & -0.18 \\ -0.21 & -0.2 & -0.09 & -2.63 \\ 0.91 & 1.56 & 1.67 & -1.13 \\ -1.06 & -1.32 & -1.08 & 0.17 \\ 0.44 & 0.04 & -0.6 & -2.46 \\ -0.26 & 0.11 & 0.64 & 3.08 \end{bmatrix}$$

$$C = \begin{bmatrix} 0.04 & 0.73 & 0.03 & 0 & -0.02 & 0 \\ 0 & 0.63 & -0.43 & 0.07 & -1.06 & -0.09 \\ -0.09 & 0.44 & -1.36 & 0.06 & -0.56 & -0.12 \\ -0.13 & 0.34 & -1.79 & -0.05 & 0.1 & 0.03 \\ -0.21 & 0.03 & 0.03 & 0.01 & -0.05 & -0.13 \\ -0.23 & -0.04 & -0.3 & -0.03 & -0.72 & -0.21 \\ -0.28 & -0.19 & -1.01 & -0.5 & -0.32 & -0.15 \\ -0.29 & -0.29 & -1.32 & -1.09 & 0.07 & 0.64 \end{bmatrix}$$

$$D = \begin{bmatrix} 0 \end{bmatrix}.$$